

Electronic Supplementary Material (ESI) for New Journal of Chemistry.

Supporting Information

An off-on-off fluorescence probe based on pyrazole derivative for Al³⁺ and Fe³⁺

Kehui Wei^a, Sheyun Lyu^b, Yuanying Liu^a, Mingyi Kang^a, Peng Liu^a, Xiaofeng Yang^a, Meishan Pei^a
and Guangyou Zhang^{a,*}

^a School of chemistry and chemical engineering, University of Jinan, Jinan 250022, China. E-mail address: chm_zhanggy@ujn.edu.cn.

^b Henan Sanmenxia Aoke Chemical Industry Co. Ltd., Sanmenxia 472000, China. E-mail address: lsy13525237769@163.com.

***Corresponding author:** Guangyou Zhang, E-mail address: chm_zhanggy@ujn.edu.cn.

Table of Contents

1. **Figure. S1.** ^1H NMR spectra of compound **L**.
2. **Figure. S2.** ^{13}C NMR spectra of compound **L**.
3. **Figure. S3.** FTIR spectra of compound **L**.
4. **Figure. S4.** ESI-MS spectra of compound **L**.
5. **Figure. S5.** UV-vis absorption spectra of **L** upon addition of various metal ions.
6. **Figure. S6.** Benesi-Hildebrand curve assuming 1:2 stoichiometry for association between **L** and Al^{3+} .
7. **Figure. S7.** Absorption spectrum of **L** (1×10^{-5} M) with increasing addition of Al^{3+} (0-15 equiv.).
8. **Figure. S8.** Switching cycles of fluorescence intensity of **L** aqueous solutions at 503 nm by alternate addition of Al^{3+} and PPI.
9. **Figure. S9.** Benesi-Hildebrand curve assuming 1:2 stoichiometry for association between $\text{L}[\text{Al}^{3+}]$ and Fe^{3+} .
10. **Figure. S10.** Absorption spectrum of $\text{L}[\text{Al}^{3+}]$ with increasing addition of Fe^{3+} (0-25 equiv.).
11. **Figure. S11.** The fluorescence intensity of $\text{L}[\text{Al}^{3+}]$ towards Fe^{3+} in the presence of other metal ions.
12. **Figure. S12.** UV-vis absorption spectra of $\text{L}[\text{Al}^{3+}]$ upon addition of various metal ions.
13. **Figure. S13.** Job's Plot of **L** with Al^{3+} in DMSO/ H_2O buffer solution ($v/v = 9/1$, tris = 10 mM, pH = 7.4).
14. **Figure. S14.** Job's Plot of $\text{L}[\text{Al}^{3+}]$ with Fe^{3+} in DMSO/ H_2O buffer solution ($v/v = 9/1$, tris = 10 mM, pH = 7.4).
15. **Fig. S15.** ESI-MS of compound **L** with addition of Al^{3+} .
16. **Fig. S16.** ESI-MS of compound **L** with addition of Fe^{3+} .

17. **Fig. S17.** FTIR of compound **L** with addition of Al^{3+} .
18. **Fig. S18.** The optimized geometry of **L**, $\text{L}[\text{Al}^{3+}]$ and $\text{L}[\text{Fe}^{3+}]$.
19. **Table S1.** Comparison to this work with the published sensors for Al^{3+} detection.
20. **Table S2.** Comparison to this work with the published sensors for Fe^{3+} detection.
21. **Table S3.** Optical properties of **L** in the absence/presence of Al^{3+} or Fe^{3+} .
22. **Table S4.** Determination of **L** to Al^{3+} and Fe^{3+} in tap water.

Calculation of quantum yield

The quantum yield was calculated according to the following formula (1):

$$\Phi_u = \Phi_s \frac{F_u A_s n_u^2}{F_s A_u n_s^2} \quad (1)$$

Φ , F , A , and n represent the quantum yield, the integrated area under the corrected emission spectra, the absorbance intensity at the excitation wavelength and the refractive index of solvent, respectively. In addition, s refers to rhodamine B as the standard, and u refers to the target. The quantum yield (Φ) of rhodamine B dissolved in anhydrous ethanol is 0.97.

Calculation of detection limit

The detection limits of **L** for Al^{3+} were calculated by the following formula (2):

$$LOD = 3\sigma/s \quad (2)$$

where σ is the standard deviation of 10 times the intensity of free **L** ($\text{L}[\text{Al}^{3+}]$, $\text{L}[\text{Fe}^{3+}]$), and s is the slope of the emission intensity of **L** ($\text{L}[\text{Al}^{3+}]$, $\text{L}[\text{Fe}^{3+}]$) as a function of the Al^{3+} or Fe^{3+} concentration.

Calculation of association constant

The association constant between **L** and Al^{3+} was calculated by the following formula (3) and the association constant between $\text{L}[\text{Al}^{3+}]$ and Fe^{3+} was calculated by the following formula (4):

$$\frac{1}{\Delta F} = \frac{1}{\Delta F_{max}} + \frac{1}{K\Delta F_{max}} \cdot \frac{1}{[\text{Al}^{3+}]^2} \quad (3)$$

$$\frac{1}{\Delta F} = \frac{1}{\Delta F_{max}} + \frac{1}{K\Delta F_{max}} \cdot \frac{1}{[\text{Fe}^{3+}]^2} \quad (4)$$

where $\Delta F = F - F_0$ and $\Delta F_{max} = F_{max} - F_0$.

with F_0 , F and F_{max} being the fluorescence intensities of the free **L**, at various concentration of Al^{3+} and at the maximum concentration of Al^{3+} respectively.

with F_0 , F and F_{max} being the fluorescence intensities of the $\text{L}[\text{Al}^{3+}]$, at various concentration of Fe^{3+}

and at the maximum concentration of Fe^{3+} respectively.

Theoretical calculation

Density functional theory (DFT) structure optimization was performed using the Gaussian 09 program. In all cases, the structures were optimized using the B3LYP functional and the mixed basis set 6-31+G(d). For all optimized structures, frequency calculations were performed to confirm the absence of imaginary frequencies. Subsequently, TD-DFT calculations were performed based on B3LYP/6-31G* and B3LYP/LANL2DZ to obtain the corresponding molecular orbitals and energy calculations. According to the calculation results of DFT/TD-DFT, the reaction mechanism of **L** with Al^{3+} and Fe^{3+} ions was further proposed.

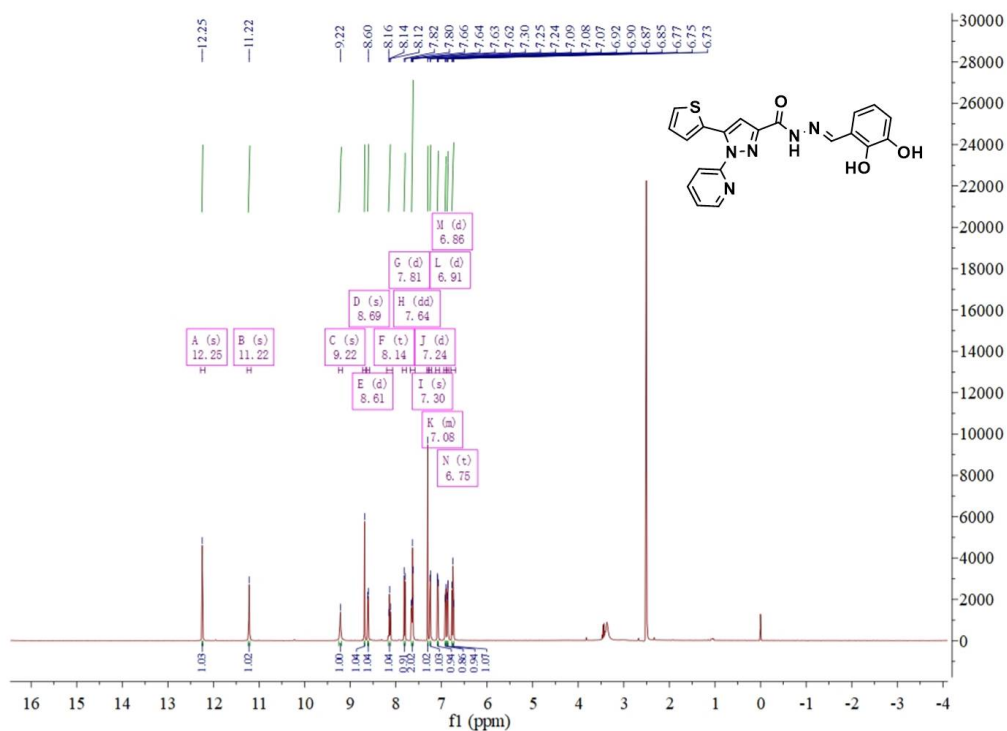


Fig. S1 ^1H NMR spectra of compound L.

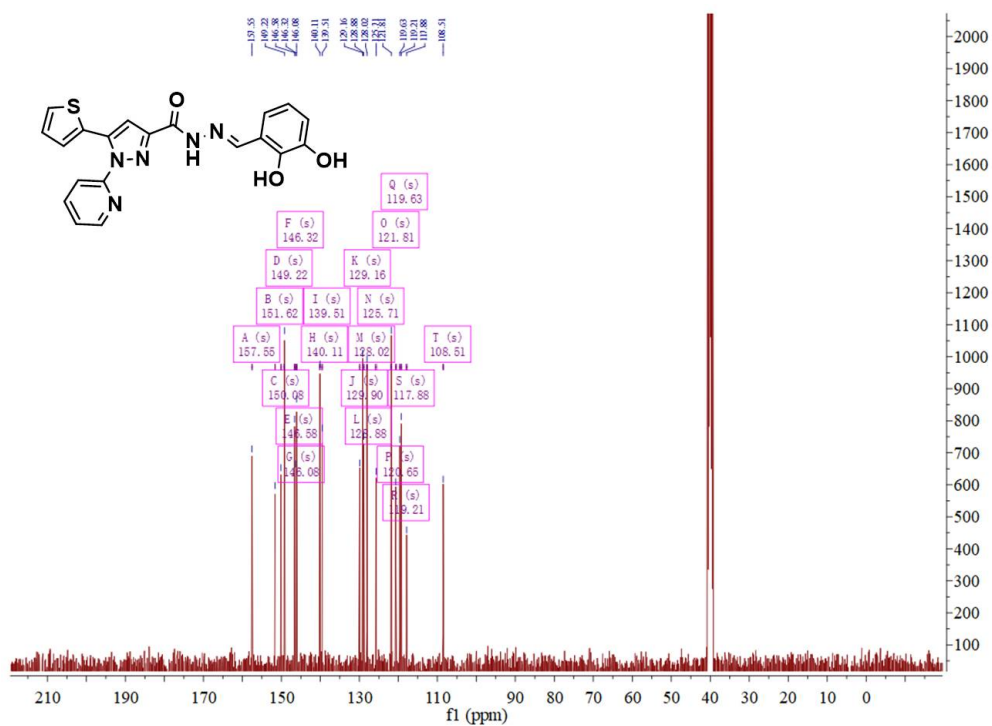


Fig. S2 ^{13}C NMR spectra of compound L.

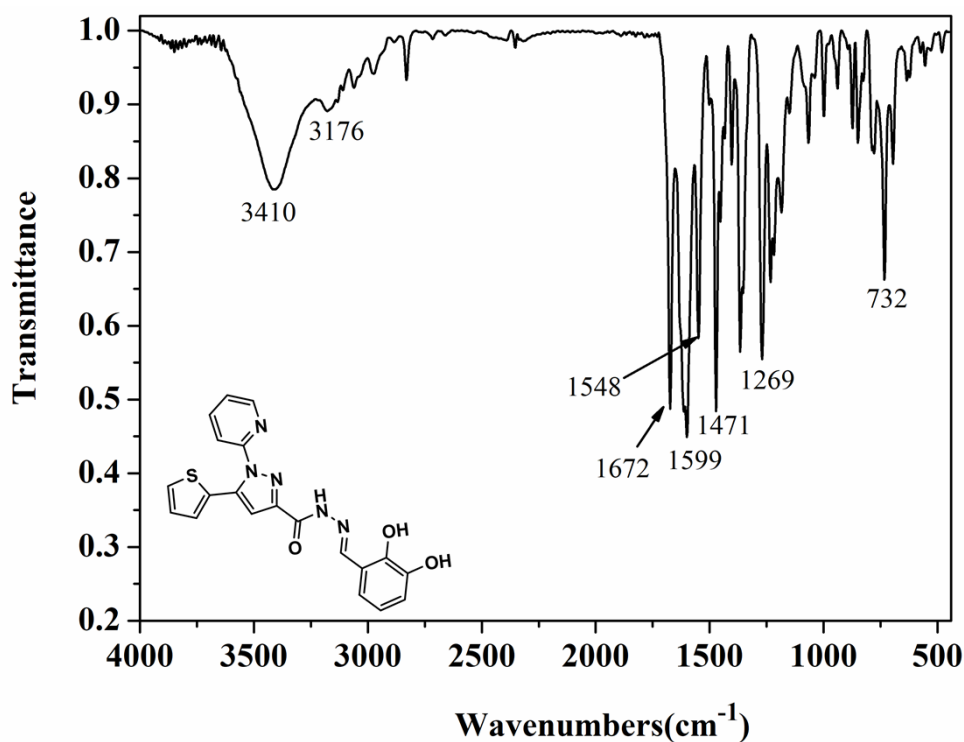


Fig. S3 FTIR spectra of compound L.

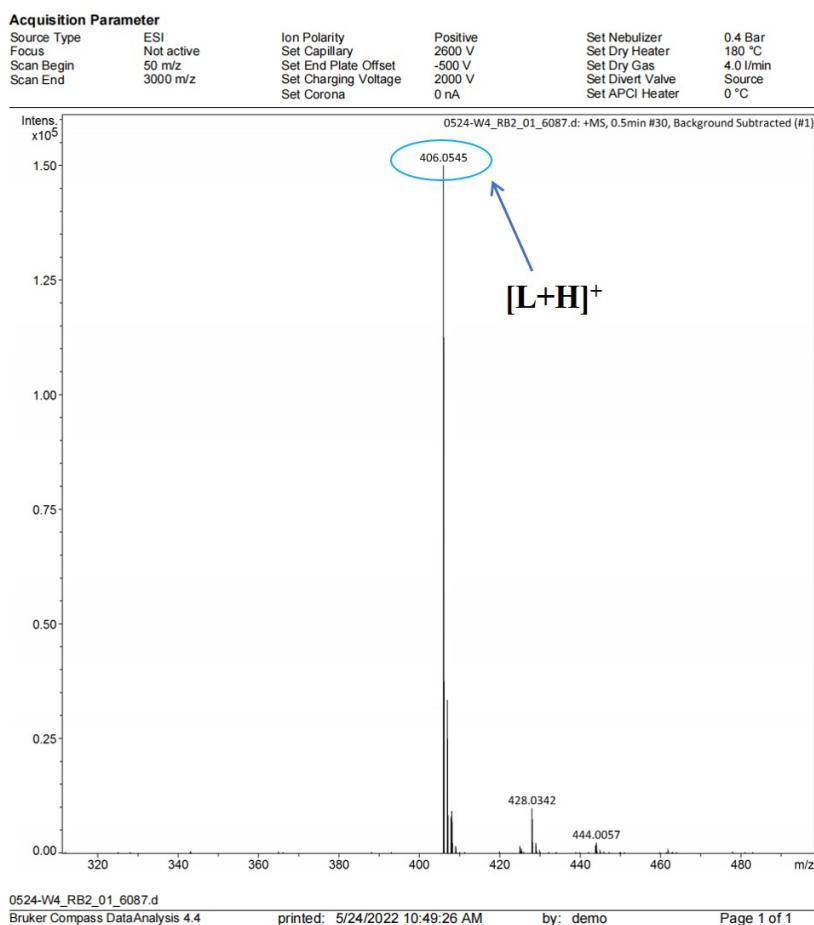


Fig. S4 ESI-MS spectra of compound L.

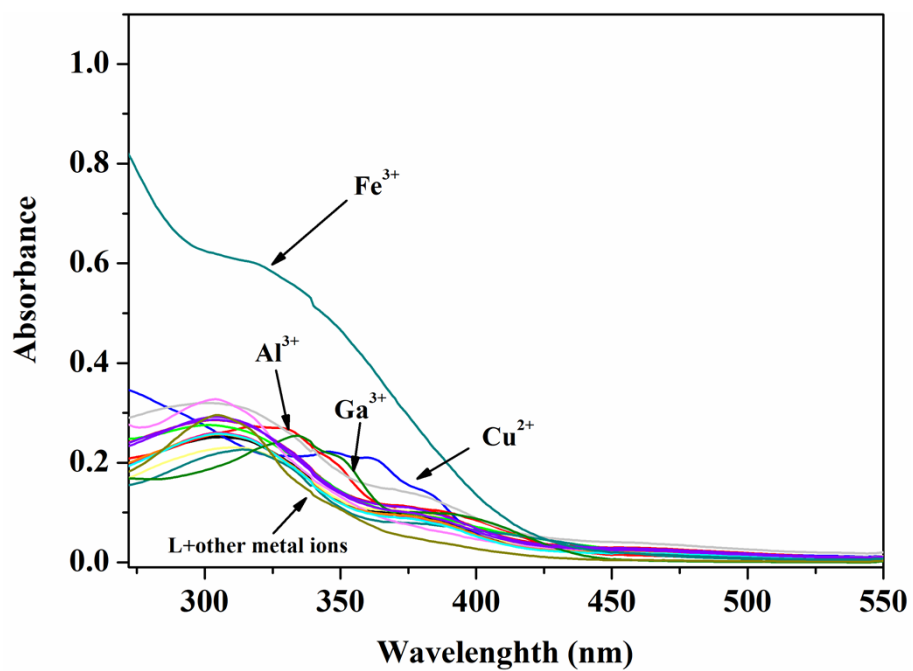


Fig. S5 UV-vis absorption spectra of L upon addition of various metal ions.

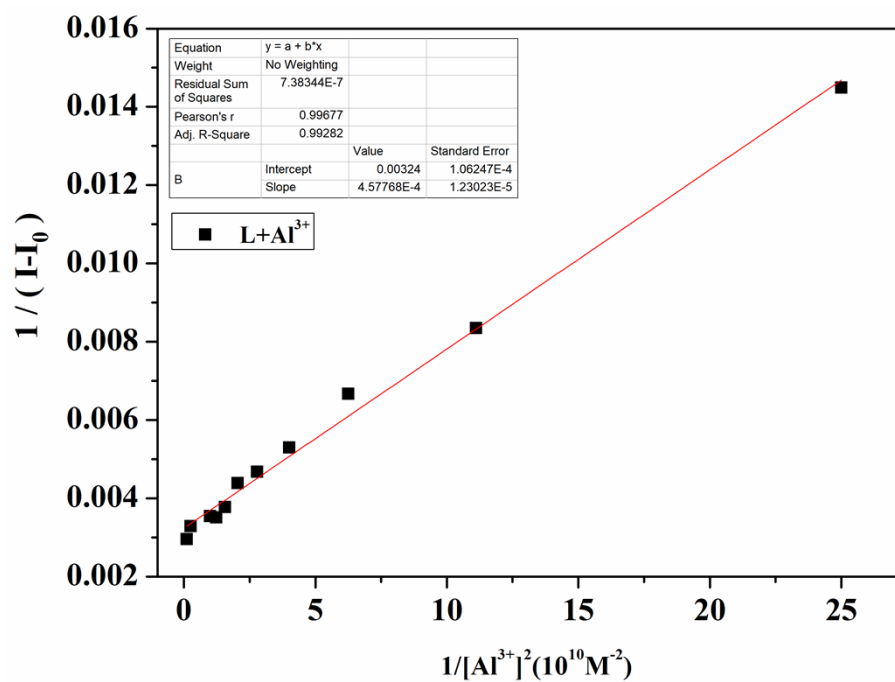


Fig. S6 Benesi-Hildebrand curve assuming 1:2 stoichiometry for association between L and Al³⁺.

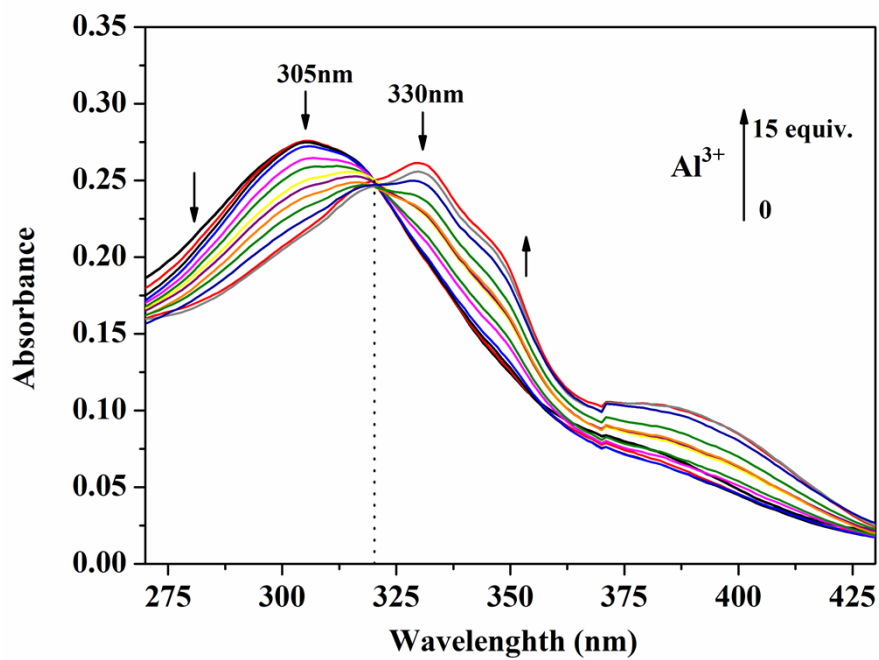


Fig. S7 Absorption spectrum of L (1×10^{-5} M) with increasing addition of Al³⁺ (0-15 equiv.).

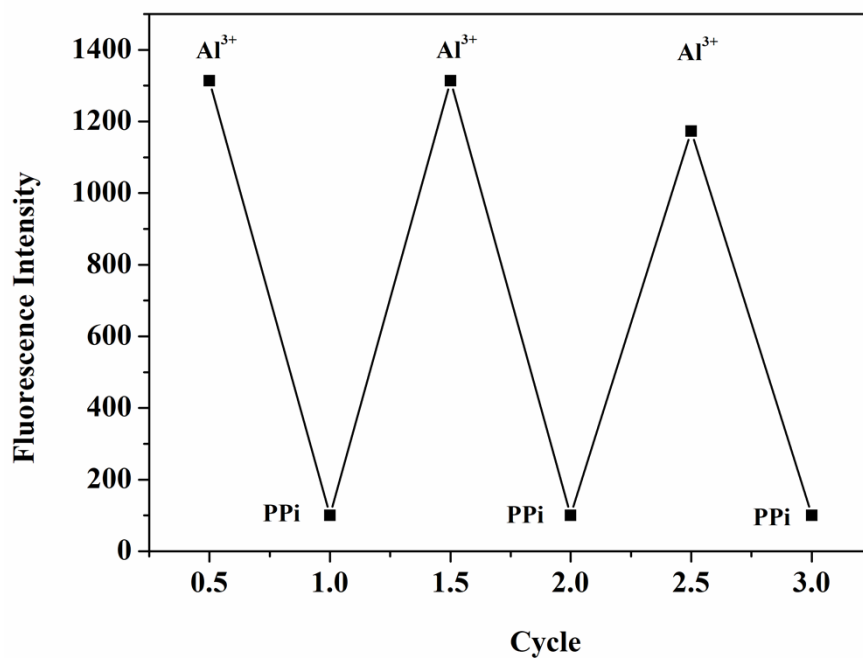


Fig. S8 Switching cycles of fluorescence intensity of L aqueous solutions at 503 nm by alternate addition of Al³⁺ and PPI.

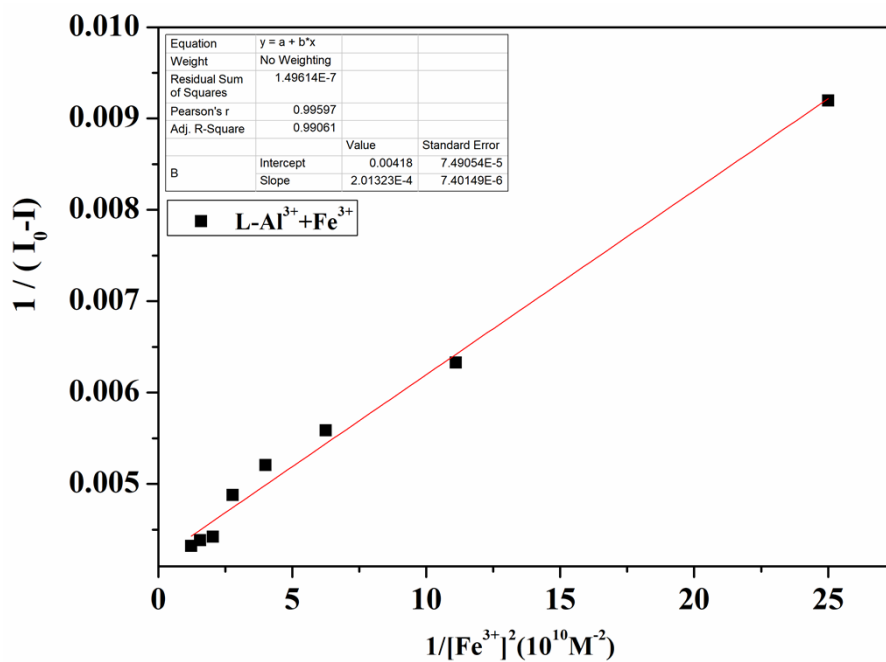


Fig. S9 Benesi-Hildebrand curve assuming 1:2 stoichiometry for association between L[Al³⁺] and Fe³⁺.

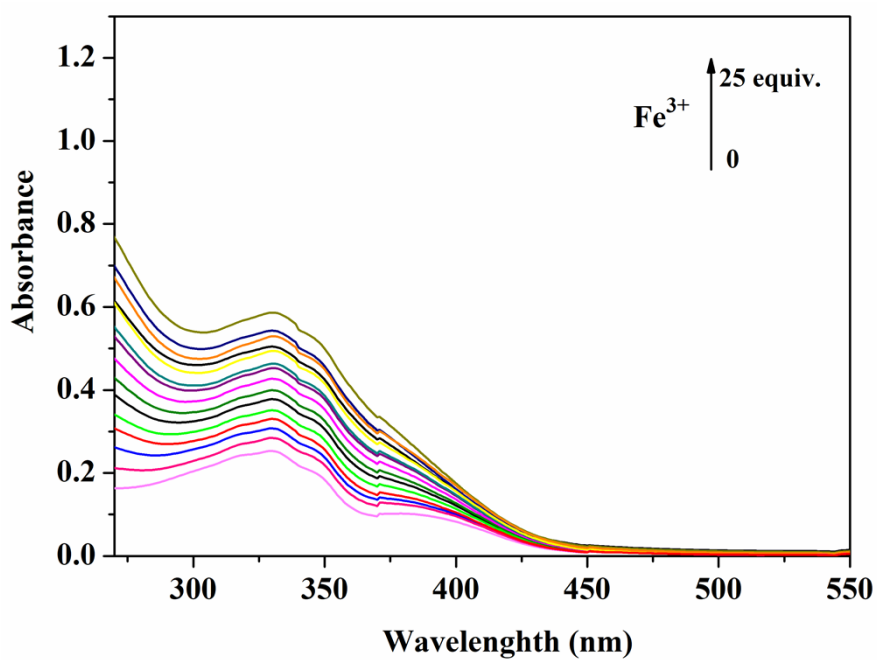


Fig. S10 Absorption spectrum of L[Al³⁺] with increasing addition of Fe³⁺ (0-25 equiv.).

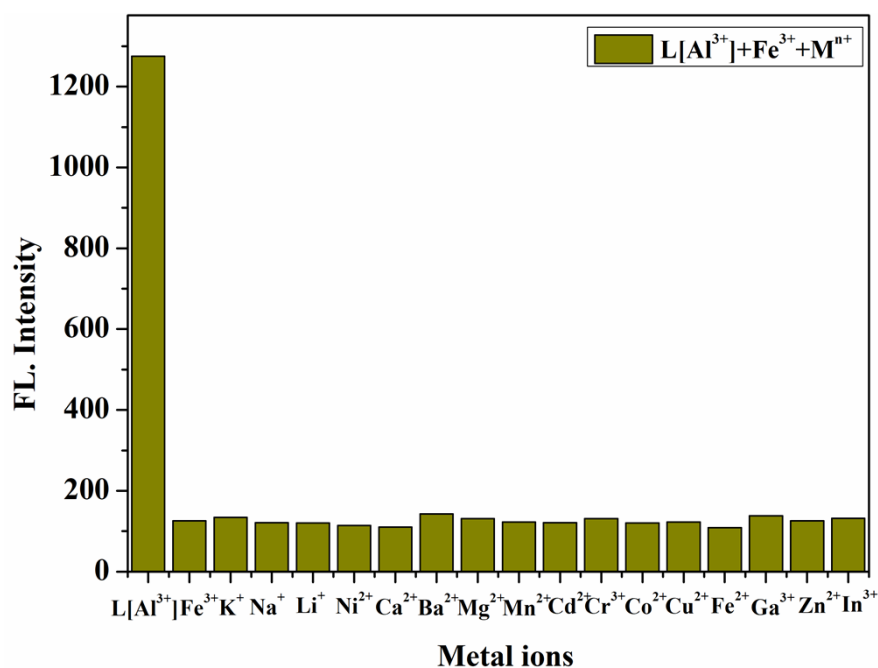


Fig. S11 The fluorescence intensity of L[Al³⁺] towards Fe³⁺ in the presence of other metal ions.

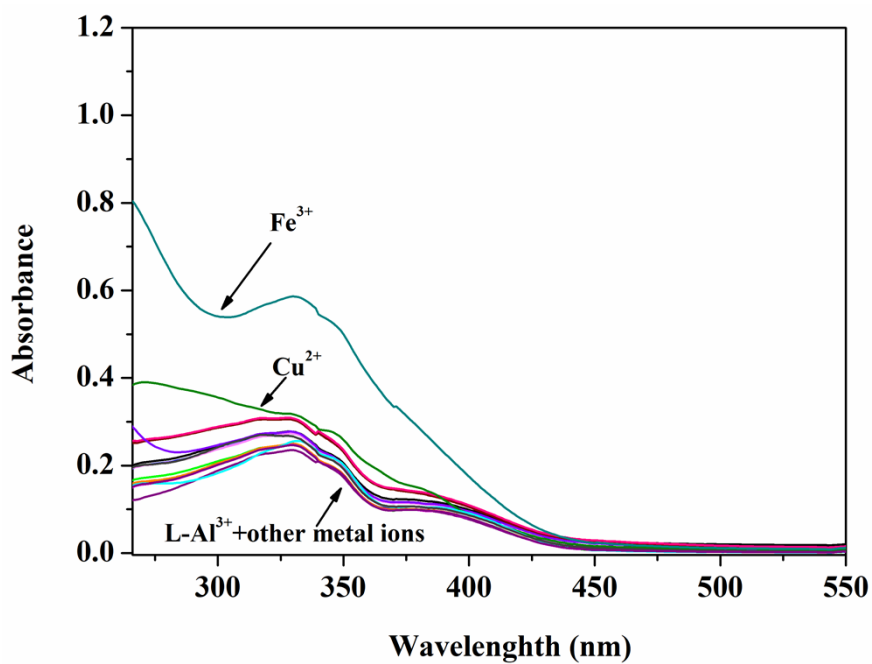


Fig. S12 UV-vis absorption spectra of L[Al³⁺] upon addition of various metal ions.

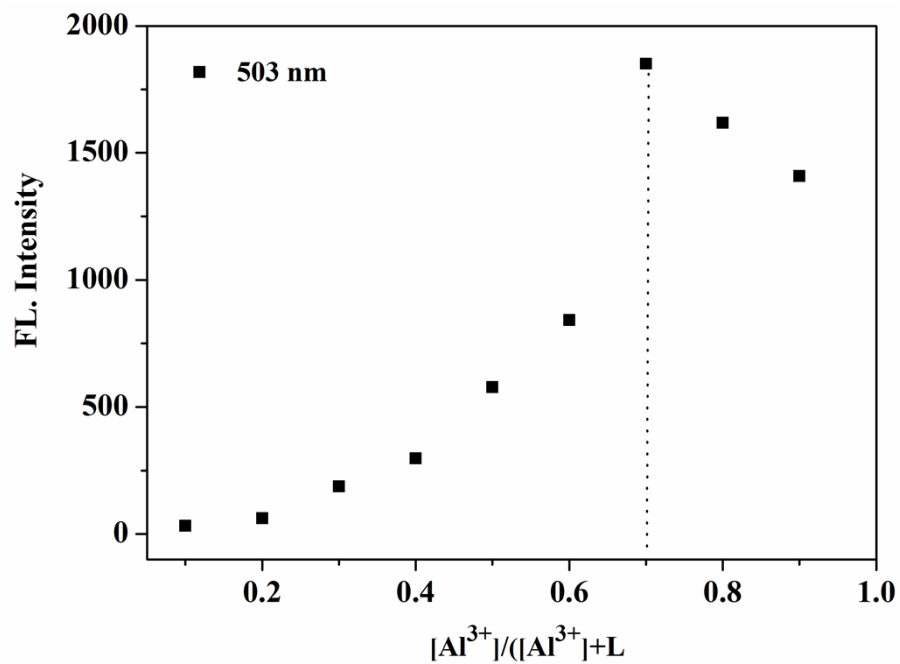


Fig. S13 Job's Plot of L with Al^{3+} in DMSO/ H_2O buffer solution (v/v = 9/1, tris = 10 mM, pH = 7.4).

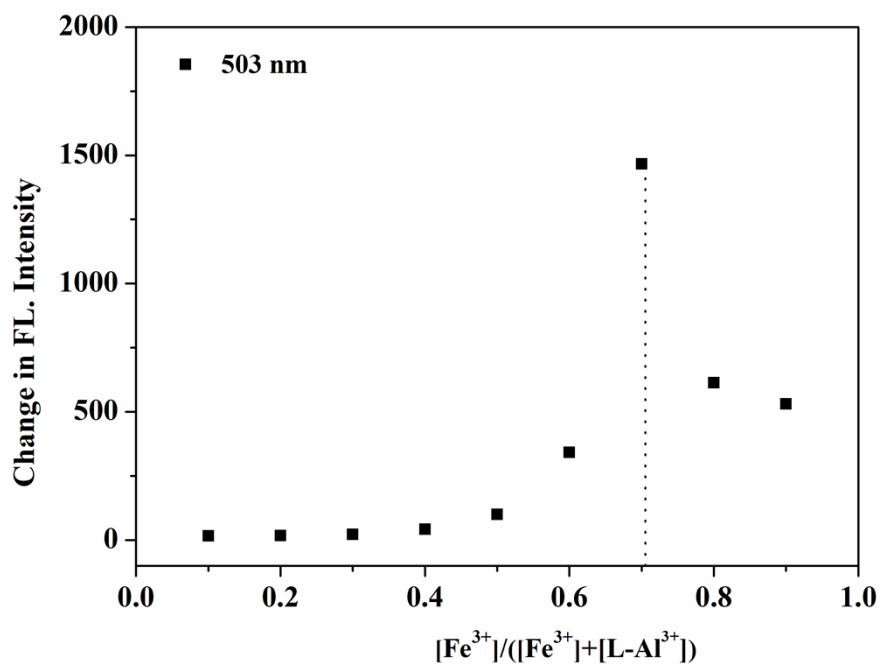


Fig. S14 Job's Plot of $L[Al^{3+}]$ with Fe^{3+} in DMSO/ H_2O buffer solution (v/v = 9/1, tris = 10 mM, pH = 7.4).

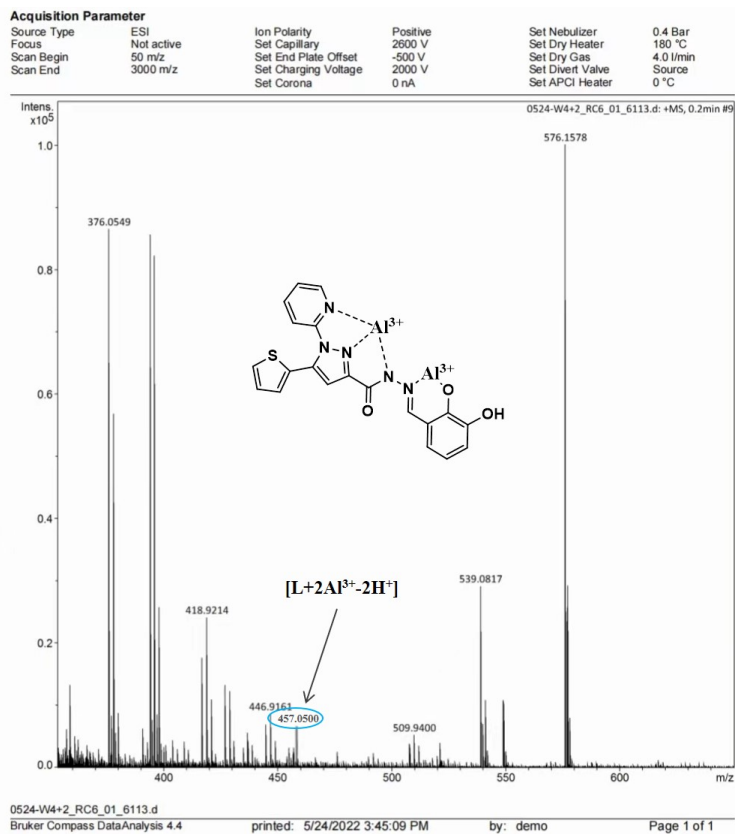


Fig. S15 ESI-MS of compound **L** with addition of Al^{3+} .

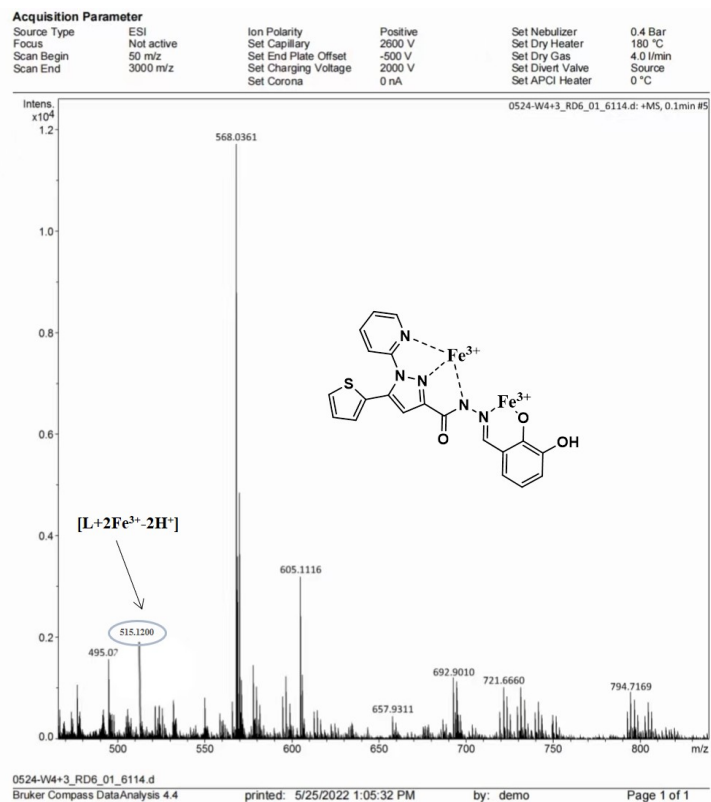


Fig. S16 ESI-MS of compound **L** with addition of Fe^{3+} .

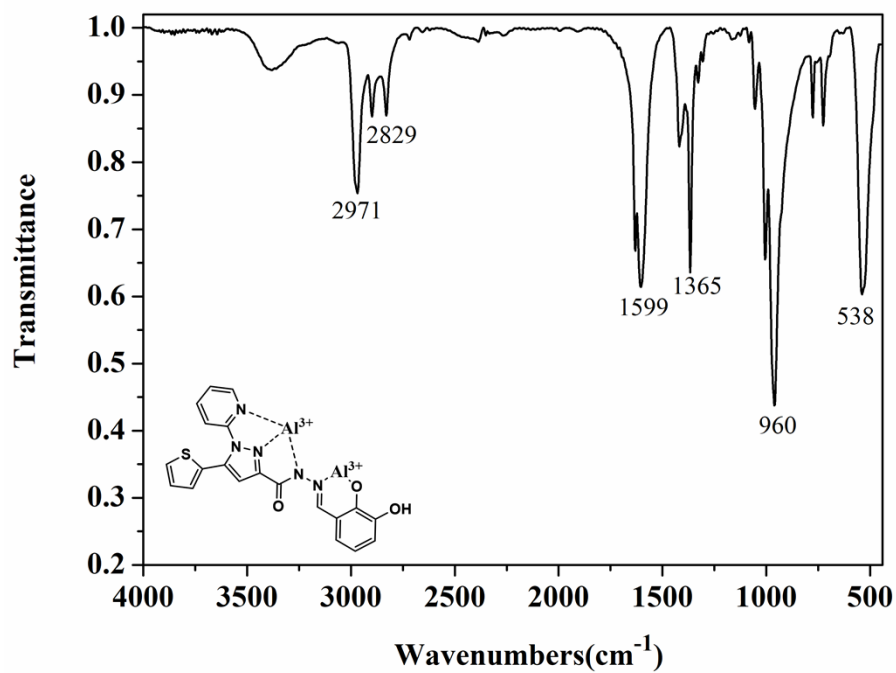


Fig. S17 FTIR of compound L with addition of Al^{3+} .

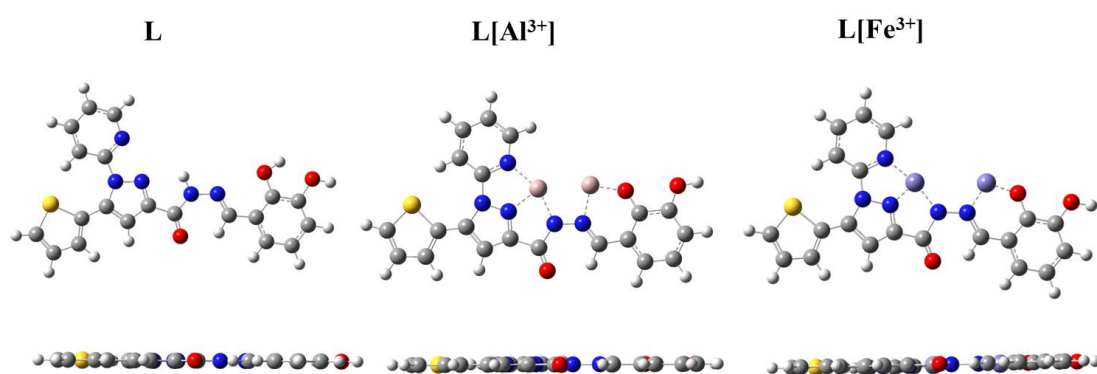
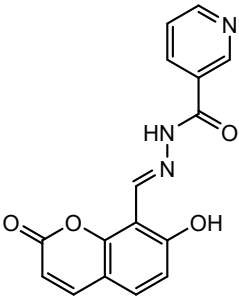
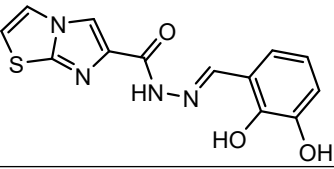
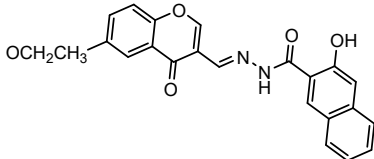
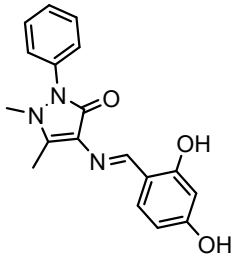
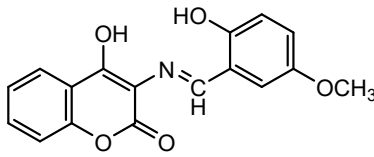
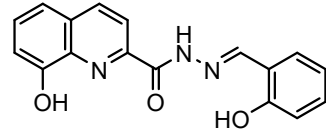
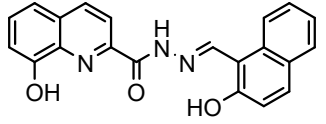


Fig. S18 The optimized geometry of L, $\text{L}[\text{Al}^{3+}]$ and $\text{L}[\text{Fe}^{3+}]$.

Table S1. Comparison to this work with the published sensors for Al³⁺ detection.

Sensors	Detection process	Detection limit	Solvent Media	References
	turn-on	2.51×10^{-7} M	EtOH-HEPES (95:5, v/v)	[2]
	turn-on	3.57×10^{-8} M	DMF-H ₂ O (1:1, v/v)	[4]
	turn-on	1.82×10^{-7} M	MeOH-H ₂ O (3:1, v/v)	[7]
	turn-on	6.1×10^{-8} M	EtOH	[8]
	turn-on	1.62×10^{-6} M	MeOH-HEPES Buffer (9:1, v/v)	[9]
 	turn-on	1.48×10^{-8} M 4.23×10^{-8} M	DMSO-H ₂ O (1/2, v/v)	[10]

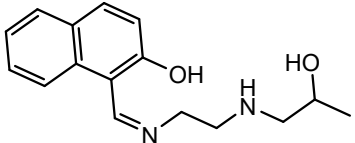
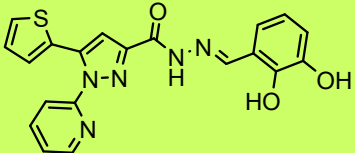
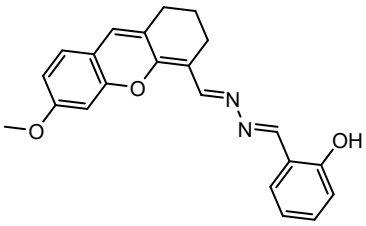
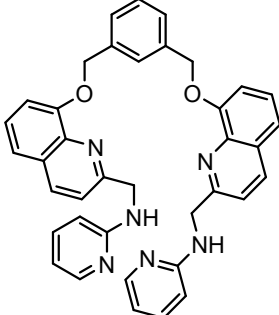
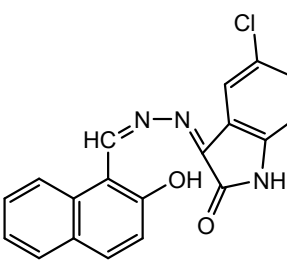
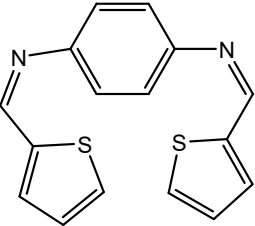
	turn-on	$1.8 \times 10^{-7} \text{ M}$	MeOH	[11]
	/	$1.1 \times 10^{-8} \text{ M}$	DMSO-H ₂ O (9:1, v/v)	This work

Table S2. Comparison to this work with the published sensors for Fe³⁺ detection.

Sensors	Detection process	Detection limit	Solvent Media	References
	turn-on	$9.83 \times 10^{-8} \text{ M}$	MeCN-Tris (2/1, v/v)	[13]
	turn-off	$1.96 \times 10^{-5} \text{ M}$	DMF-Tris (1/1, v/v)	[16]
	turn-off	$1.37 \times 10^{-8} \text{ M}$	DMSO-H ₂ O (v/v = 3/7)	[17]
	turn-on	$3.8 \times 10^{-7} \text{ M}$	/	[18]

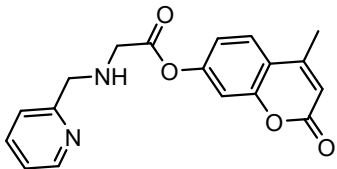
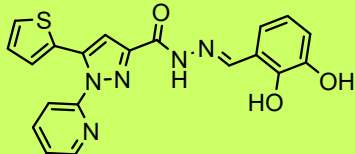
	turn-off	3.2×10^{-7} M	H ₂ O	[21]
	/	4.45×10^{-8} M	DMSO/H ₂ O (9:1, v/v)	This work

Table S3. Optical properties of **L** in the absence/presence of Al³⁺ or Fe³⁺.

Compound	Quantum Yield	LOD	Association Constant
L	0.071	\	\
L [Al ³⁺]	0.26	1.1×10^{-8} M	1.84×10^{10} M ⁻²
L [Fe ³⁺]	0.0021	4.45×10^{-8} M	4.80×10^{10} M ⁻²

Table S4. Determination of **L** to Al³⁺ and Fe³⁺ in tap water

Ion	Sample	Ion added (mol L ⁻¹)	Ion recovered (mol L ⁻¹)	Recovery (%)	RSD (%)
Al ³⁺	1	1×10^{-5}	1.04×10^{-5}	104.00	0.95
	2	2×10^{-5}	1.92×10^{-5}	96.00	0.52
	3	3×10^{-5}	3.02×10^{-5}	100.67	0.33
Fe ³⁺	1	1×10^{-5}	1.12×10^{-5}	112.00	0.86
	2	2×10^{-5}	1.94×10^{-5}	97.00	0.49
	3	3×10^{-5}	3.04×10^{-5}	101.30	0.32